


Article

Lineal Energy of Proton in Silicon by a Microdosimetry Simulation

Yueh Chiang ¹, Cher Ming Tan ^{2,3,4}, Chuan-Jong Tung ^{1,5}, Chung-Chi Lee ^{1,5} and Tsi-Chian Chao ^{1,5,*}

¹ Department of Medical Imaging and Radiological Sciences, College of Medicine, Chang Gung University, Kwei-Shan, Tao-Yuan 333, Taiwan; D0503203@cgu.edu.tw (Y.C.); cjtung@mail.cgu.edu.tw (C.-J.T.); ccle@mail.cgu.edu.tw (C.-C.L.)

² Center for Reliability Sciences and Technologies, Chang Gung University, Kwei-Shan, Tao-Yuan 333, Taiwan; cmtan@cgu.edu.tw

³ Center for Reliability Engineering, Mingchi University of Technology, New Taipei City 243, Taiwan

⁴ Department of Urology, Chang Gung Memorial Hospital, Linkou 333, Taiwan

⁵ Particle Physics and Beam Delivery Core Laboratory, Institute for Radiological Research, Chang Gung University/Chang Gung Memorial Hospital, Linkou, Kwei-Shan, Tao-Yuan 333, Taiwan

* Correspondence: chaot@mail.cgu.edu.tw

Abstract: Single event upset, or Single Event Effect (SEE) is increasingly important as semiconductor devices are entering into nano-meter scale. The Linear Energy Transfer (LET) concept is commonly used to estimate the rate of SEE. The SEE, however, should be related to energy deposition of each stochastic event, but not LET which is a non-stochastic quantity. Instead, microdosimetry, which uses a lineal calculation of energy lost per step for each specific track, should be used to replace LET to predict microelectronic failure from SEEs. Monte Carlo simulation is used for the demonstration, and there are several parameters needed to optimise for SEE simulation, such as the target size, physical models and scoring techniques. We also show the thickness of the sensitive volume, which also correspond to the size of a device, will change the spectra of lineal energy. With a more comprehensive Monte Carlo simulation performed in this work, we also show and explain the differences in our results and the reported results such as those from Hiemstra et al. which are commonly used in semiconductor industry for the prediction of SEE in devices.

Keywords: single event effect; Monte Carlo simulation; microdosimetry; linear energy transfer; lineal energy



Citation: Chiang, Y.; Tan, C.M.; Tung, C.-J.; Lee, C.-C.; Chao, T.-C. Lineal Energy of Proton in Silicon by a Microdosimetry Simulation. *Appl. Sci.* **2021**, *11*, 1113. <https://doi.org/10.3390/app11031113>

Academic Editor: Carosena Meola

Received: 29 December 2020

Accepted: 22 January 2021

Published: 26 January 2021

Publisher's Note: MDPI stays neutral with regard to jurisdictional claims in published maps and institutional affiliations.



Copyright: © 2021 by the authors. Licensee MDPI, Basel, Switzerland. This article is an open access article distributed under the terms and conditions of the Creative Commons Attribution (CC BY) license (<https://creativecommons.org/licenses/by/4.0/>).

1. Introduction

Radiations exist around us in the air, and it includes photon, electron, neutron and alpha particle. These radiations are critical traditionally in the aerospace applications because they could render function loss for the satellites and even lead to material degradation [1], and they can be ignored at the sea level. However, as microelectronic devices are scaling down aggressively with the advancement in semiconductor technology, nano-meter devices are now susceptible to these radiations, and they can no longer be overlooked. These radiations can interact with semiconductor devices and cause damages to the devices or functional errors to their associated circuits [2].

The effect of these radiations on microelectronic devices can be categorized into two different effects, namely a cumulative effect termed as Total Ionization Dose (TID) effect, and a stochastic effect, termed as Single Event Effect (SEE) [3]. SEE describes the event of electronic device malfunction or failure caused by “single” radiation hits. SEE is critical for devices where their rebooting is difficult or even impossible, and examples of such devices are pacemakers, autopilot systems, and microelectronics used in space missions. Lineal Energy Transfer (LET) is widely used as a key index for SEE prediction [4,5].

LET is a non-stochastic quantity which gave an expectation value of energy imparted from particle to a local site. International Commission on Radiation Units and Measure-

ments (ICRU) gave the definition of LET of a particle (Equation (1)) in its report 16 [6] as the quotient of dE by dl , where dl is the distance traversed by this particle and dE is the mean energy-loss owing to collisions with energy transfers less than some upper limit Δ , which is the cut off energy of delta ray.

$$L_{\Delta} = \left(\frac{dE}{dl} \right)_{\Delta} \quad (1)$$

There is a long history of studies on LET in microelectronic applications. O'Neill et al. conducted a series of studies on LET with secondary ions generated by the irradiation of silicon with protons, and they showed that proton testing is suitable to screen microelectronic devices for low earth orbit susceptibility to heavy ions [7]. Hiemstra et al. provided the LET spectra of protons in 50–500 MeV, which are commonly used for SEE testing, and gave the scaled factor of proton fluence for Geosynchronous orbits by a simplified Monte Carlo simulation [8]. Biersack and Ziegler carried out a comprehensive study of the ion ranges and stopping powers in solids and provide a useful toolkit called Stopping and Range of Ions in Matter (SRIM). This toolkit allows the radiation particles to be modelled in a simple microelectronic structure [9,10].

Dodd et al. provided the trend of LET thresholds of SEE with feature sizes from 1 to 0.1 μm [11]. In their results, the threshold decreases when the feature size decreases due to the following. Firstly, when the sizes of the devices are smaller, the critical charges, i.e., the amount of charges to change the performance of the devices will be smaller. Secondly, with a smaller target, the energy deposition of each specific radiation particle will have a greater deviation, and there is a chance of a huge energy deposition leading to a huge induced charge.

Single Event Rate (SER) can be directly tested under specific protocols [12] or modelled with known natural radiation environment for these cosmic rays [13]. JEDEC Solid State Technology Association give the protocol JESD57A [12] to guide the procedures for the SEE tests. These tests are usually expensive and difficult. Another way to predict single event rate is to convolute the LET spectra in target orbital with the single event cross sections (either for a device or averaged per bit) from either experiment or simulation. In this method, single event cross sections versus LET is usually a single value function. Warren used a set of heavy ion with specific kinetic energy to derive the single event cross sections and predict the single event upset rate of a 0.25 μm CMOS SRAM well [14].

As the feature size reduced to a few nanometres, this “single-value assumption” may no longer valid. Warren et al. found that in a 90 nm CMOS irradiated with heavy ions, although the effective LET is the same, the single event cross sections can have more than three order of magnitude differences [15]. In other words, LET distributions can be different in various feature sizes of the devices under an exact irradiation condition. With today nano-meter microelectronic devices, the variability of LET from a given radiation can be very large, and this leads to the necessity to use the concept of lineal energy distribution to predict SEE in a given device.

In fact, LET is commonly used in the cm/mm scale for deterministic events. For microelectronics, microdosimetry is more appropriate to describe the stochastic events. Down to nanometre scale, many researchers used realistic track structure to predict local effect of different radiations [16–19]. This track structure approach will be practical in the simulation, but it is still difficult to compare with measurements. In addition, these track structure codes can only simulate interactions in limited materials and semiconductor materials is yet to be included. Furthermore, the track structure will only be meaningful when detailed geometry of a specific microelectronic device is given. On the other hand, microdosimetry is easier to be modelled for radiation effect prediction [20]. We have used this microdosimetry approach to investigate the equivalence of neutrons and protons in SEEs testing [21].

ICRU report 16 considered that the local energy density and individual event size will be more relevant than LET for microscopic structures [6]. These concepts of local

energy density and individual event size have been clarified in the ICRU report 36 for the introduction of microdosimetry [22]. The basic concepts of microdosimetry are developed by Rossi and co-workers [23,24], and they used two stochastic quantities, specific energy (z) and lineal energy (y) to replace dose and LET. Lineal energy (y) of microdosimetry is a way to estimate radiation quality/impact microscopically [22], and it is defined as,

$$y = \frac{\varepsilon}{\bar{l}} = \frac{\sum_i \varepsilon_i}{\bar{l}} \quad (2)$$

where the parameters in the equation is defined below.

When a radiation particle enters a target, it will interact with the target material along its track in the material. Energy deposit ε_i is defined as the energy deposited in i^{th} "Single" interaction. The sum of the ε_i in the target within one track is defined as the energy imparted (ε). Mean chord length (\bar{l}) is the mean length of randomly oriented chords in a given volume [22].

In large size target, the number of interactions will be large, and the distribution of y will converge to an expected value, which is LET. However, at the nanometric scale, the number of interactions is small, and only very few interaction events occur in a radiation track. Thus, y would have a wide distribution. In this case, providing discrete values of LET will be meaningless because different y values would have different contributions to SEEs and the relationship is non-linear.

Monte Carlo simulation is commonly used in microdosimetry studies [25,26], and it relies on many physical models among which nuclear interaction physics is the most important for microdosimetry study on SEE. However, a Monte Carlo simulation with detailed nuclear interaction is very time and computation resources consuming. When computing power was expensive in the past, secondary particles generation and their transport in silicon could not be included in the simulation. For example, Hiemstra et al. tried to use a simplified Monte Carlo method, which allow only one filial of secondary particles to compute their corresponding ranges. They then used the range to calculate LET and predict SEE [8]. However, the secondary particles generated under proton irradiation are usually quite unstable and will decay or have further interactions with silicon, which may generate light ions with lower energy and higher stopping powers. All these ions can affect the SEE. An example of such can be found by Ying et al. who found that carbon ions can fragment into several secondary particles during transportation [27].

Recently, there is an increasing number of Monte Carlo based SEE evaluation toolkits. Intel developed the Intel Radiation Tool (IRT) based on Geant4 [28]. Reed and colleagues in Vanderbilt University has also developed another Geant4 based Monte Carlo Radiative Energy Deposition (MRED) Code [29]. In Geant4 Space Users' Workshop and Nuclear & Space Radiation Effects Conference (NSREC), using Monte Carlo technique to predict radiation effect in semiconductor is a routine discussion. However, within the Monte Carlo framework, there are hundreds of parameters that could affect the results, and there is no conclusion on which setting is more accurate. Besides, the setting should be different for different purpose.

In this work, a Geant4 [16] based Monte Carlo simulation is performed to simulate the effect of proton beams on silicon. Different sensitive volume thicknesses are compared. The lineal energy is also analysed in detail for each particle crossing the sensitivity volume, and the physical models for intra-nuclear interaction in Geant4 are also compared.

2. Simulation Setup

The simulation in this study is based on Geant4 10.05 [16]. The physics model of electromagnetic processes in this simulation is aligned with G4EmStandardPhysics_option4. For electrons, due to their low LET, they cannot contribute to high y effects [30], and thus the step function (parameter for step size R) can be set such that R over range = 0.01 and final range = 1 nm to speed up the simulation. For hadrons that have high LET and they are therefore more important in this study, the R over range = 0.00001 and the final

range = 0.1 nm are set to improve the accuracy while keeping the efficiency of the Monte Carlo simulation.

For the intranuclear cascade, the Bertini's model is widely used [31]. The nucleon spectra from continuum-state transitions for protons on complex nuclei are calculated using the intranuclear-cascade approach. However, the model is commissioned in high-energy physics. An alternative method is a detailed three-dimensional model of the nucleus, and is based exclusively on the binary scattering between reaction participants and nucleons within this nuclear model, called binary cascade model [32]. Wright et al. showed that, at a few hundreds of MeV, the binary cascade model can predict the secondary particles yields comparable to experimental data effectively [33,34]. Additionally, there are several evaluated and experimental nuclear cross-section data banks, such as TENDL [35], EXFOR [36] and JEFF [37] which are precise but they are only for limited materials.

The intra-nuclear model, which controls secondary yields, will be compared in Geant4 using two different models. The Bertini cascade model which is widely used in SEEs studies, and the binary cascade which is found to be better for incident particles of several hundreds of MeV [34]. In addition, this work also considers the impact of high precision (HP) model using the JEFF 3.3 extension cross-section table.

The geometry in this project is a Multi-layer cylinder as shown in Figure 1. The diameter of the cylinder is 1 mm in order to ensure that most secondaries will not go out of the boundary. A 30- μm of pure silicon layer is used to generate secondary particles. Under the silicon layer is the sensitive volume (SV). The SV thickness was used to calculate lineal energy instead of mean chord length in the study. As described previously, the mean chord length concept is used better for randomly oriented chords in a given volume. The primary particles simulated in this study do not have isotropic distribution, and they are mostly incident perpendicular to the SV. Although ICRU report 36 [22] recommended using $4V/A$ to calculate mean chord length, Horowitz and Dubi [38] found that real average path length was smaller than mean chord length for non-isotropic irradiation. If we calculated mean chord length according to the $4V/A$ approach, the mean chord length of our SV with 1 mm diameter and 100 nm thickness will be 200 nm. However, the average track length in this thickness from the simulation is 104.9 nm, which is less than 5% difference to the SV thickness. Hence we use the SV thickness instead of the mean chord length to calculate y .

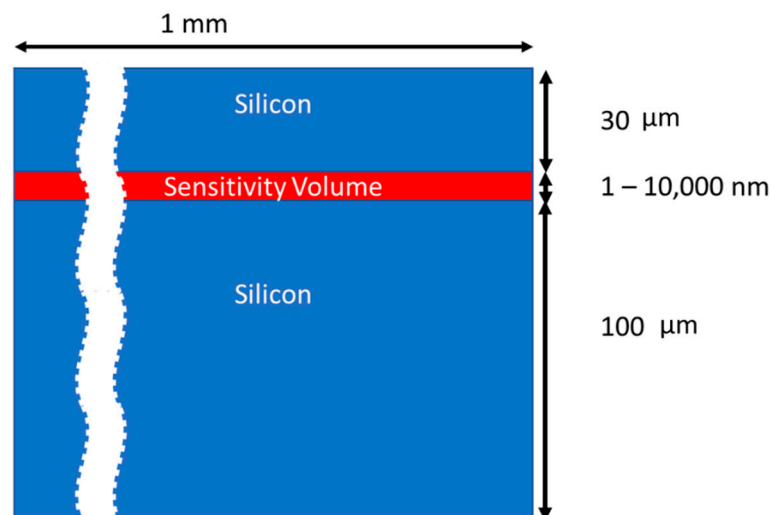


Figure 1. The geometry setup in this study. The silicon is with natural isotope abundance, density is 2330 mg/cm^3 and mean excitation potential $I = 173 \text{ eV}$.

The species and kinetic energy of each particle entering the SV are recorded as secondaries. The energies imparted from all the tracks crossing through the SV are summed up and divided by the thickness of SV to calculate the lineal energy (y). To compare the effect of SV thickness, six thicknesses, namely 1, 10, 30, 100, 1000 and 10,000 nm are simulated.

In addition, the lineal energy and secondary particle yields from the thickness of 100 nm results are further used to compared with the results from Hiemstra et al. for compatibility investigation.

For the SEEs prediction purposed, the unit of y is presented in $\text{MeV}\cdot\text{cm}^2/\text{mg}$ instead of $\text{keV}/\mu\text{m}$, which is the traditional unit in microdosimetry. In silicon, $1 \text{ MeV}\cdot\text{cm}^2/\text{mg}$ is equal to $233 \text{ keV}/\text{m}$. In conventional microdosimetry, the scale usually covers from 10^{-3} to $10^3 \text{ keV}/\mu\text{m}$. To present the entire y spectrum, semi-log scale is usually used. However, for SEEs, the LET usually is in the range of 10^{-1} to $10^2 \text{ MeV}\cdot\text{cm}^2/\text{mg}$, and differential fluence is used instead of probability density function of y .

3. Results and Discussions

3.1. Effect of SV Thickness on y Distribution

Dodd et al. [11] showed that smaller feature sizes have smaller SEE thresholds. In this study, six SV thicknesses were simulated to mimic different feature sizes. Figure 2 shows the effect of different SV thickness on the lineal energy (y) distribution. In the 10,000 nm case (green line), no secondary particle has $y > 10 \text{ MeV}\cdot\text{cm}^2/\text{mg}$. The ϵ for most secondary particles (more than 99.999%) were less than 2.33 MeV , corresponding to $1 \text{ MeV}\cdot\text{cm}^2/\text{mg}$.

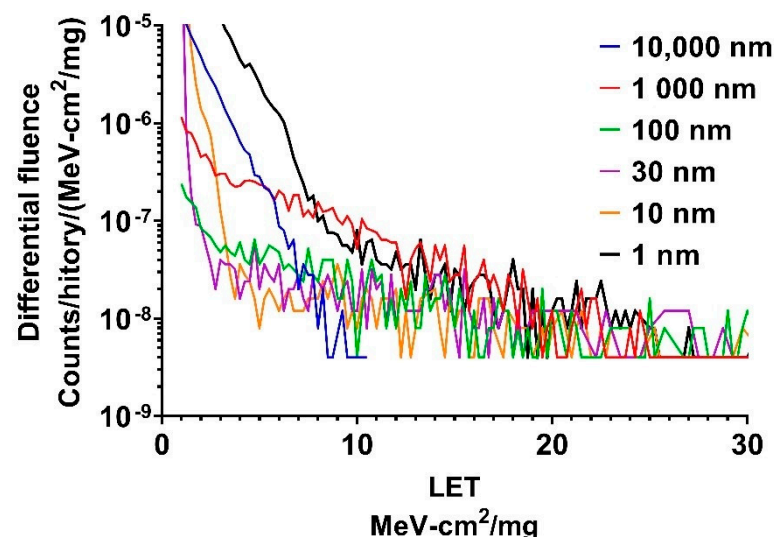


Figure 2. Lineal energy spectra of different sensitive volumes in silicon irradiated by a 200 MeV proton beam.

Let us consider the secondaries with $y > 10 \text{ MeV}\cdot\text{cm}^2/\text{mg}$ for other SV thickness. Their differential fluences decreases as the SV thickness decreases from 1000 nm to 10 nm, and this trend can be explained as follows. The y value of a particle is usually maximized when the SV thickness is close to the particle range, owing to a pronounced nature named Bragg peak. The Bragg peak describes that the heavy charged particles have little energy loss as they enter the material and then peak before the end of their path. In Figure 3, the cumulative distribution function of kinetic energy of secondary particles generated by 200 MeV proton irradiated on silicon is plotted. In this figure, more than 80% of secondary particles with atomic number (Z) larger than 2 have the kinetic energy lower than 10 MeV and 99% lower than 20 MeV. The continuous slowing down approximation (CSDA) ranges of these particles are about few thousand nm. During the slowing down process, the stopping power of particles increases as they loss their kinetic energy. The stopping power reach maximum at the end of the particle's range. When the SV size close to the particle range, it can cover the maximum stopping power. Since the particle range is approximately $1 \mu\text{m}$, the y values for the case of SV thickness = 1000 nm is larger than that for SV = 100 nm, and then 10 nm. On the other hand, when the thickness decreases to 1 nm, the differential fluences increases significantly, and the reason will be discussed later using

a CROSSER and STOPPER theory [18]. As the boundary of the CROSSER and STOPPER will be visible only at lower LET, hence this theory does not apply in this discussion where $y > 10 \text{ MeV-cm}^2/\text{mg}$.

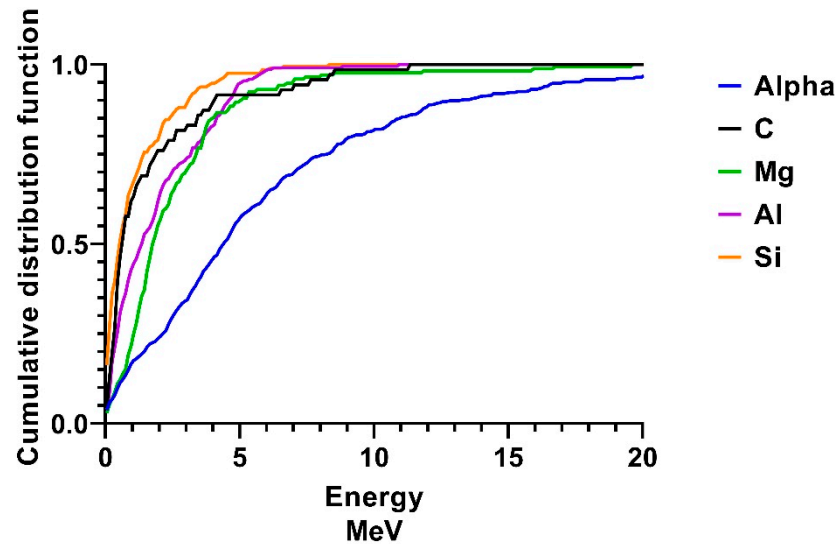


Figure 3. Cumulative distribution function of kinetic energy of secondary particles generated by 200 protons irradiated on silicon.

For the case of $y < 10 \text{ MeV-cm}^2/\text{mg}$, Figure 2 shows that the differential fluences decrease first when thickness decreased from 10,000 nm to 1000 nm, and then 100 nm. However, it increases when SV thickness continues to decrease from 100 nm to 10 nm and 1 nm. To understand the above-mentioned trends, additional SV thicknesses of 20, 40 and 50 nm are simulated respectively. Figure 4 plots the spectra in log scale, which can present the events with smaller y . In these spectra, “shoulders” can be seen for SV thickness from 10–100 nm, and the “shoulder” left shift with the SV thickness. The shoulder of 10 nm case can be found in Figure 2 which is around $y = 2\text{--}3 \text{ MeV-cm}^2/\text{mg}$. The presence of this “shoulder” can be understood from the CROSSER and STOPPER theory [18] as elaborated below.

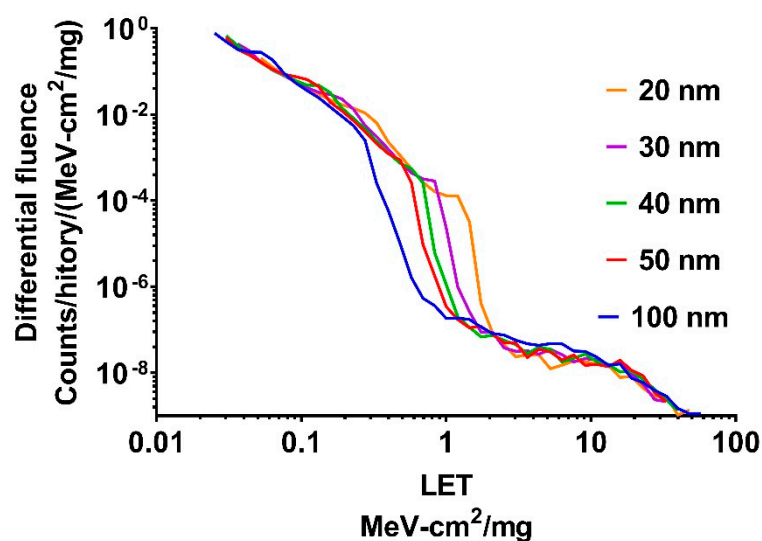


Figure 4. Lineal energy spectra of different sensitive volumes in silicon irradiated by a 200 MeV proton beam (log y scale).

When particles travel through different SVs, they can end up into either CROSSERS or STOPPERS. A CROSSER refers to particle with high enough energy that can go through the

entire SV, and a STOPPER refers to particle that stop inside SV because of its insufficient energy [18]. In Figures 2 and 4, the events on the left side of shoulder are contributed from both the CROSSER and STOOPER, but the right side can only be from the CROSSER. Since the definition of lineal energy is the energy imparted in the SV divided by the mean chord length, if the particle stopped inside the cavity, then y will be underestimated. In thicker SV, because the energy required to go through the SV is larger and more particle may become STOPPER, its y will be underestimated significantly. In Figures 2 and 4, the y -distribution of 1 nm is fairly smooth and no shoulder is observed, which means that most of the particles are CROSSER and the observed y are more realistically estimated. In SV thicker than 100 nm, the shoulder is unclear because most of the particles are STOPPERS.

Similarly, for the case of 10,000 nm, a y cut off is found and the y of heavy secondary particles is underestimated because it cannot go through the SV. In other words, the CROSSER or STOPPER theory also answers the question on the increasing differential fluence in the 1 nm case. With the shift of the shoulder to the right with decreasing SV thickness, the STOPPER becomes CROSSER, especially in the 1 nm case, and almost all particles are CROSSER.

3.2. Lineal Energy Contribution from Various Secondary Species

Since Single Event Rate (SER) is a function of LET [39], or y in this study, it is important to understand the y contribution from various secondary species for radiation hardening design. Figure 3 shows the y spectra of various types of secondary particles in pure silicon irradiated with 200 MeV protons.

The y spectra in silicon irradiated by a 200 MeV proton beam in this study was quite different from the results from Schwank [40] and Hiemstra [8]. In Schwank [40] and Hiemstra [8], their LET has a cut off around 15–16 MeV-cm²/mg. However, there are few events with y as high as 60 MeV-cm²/mg as observed in our study. Furthermore, the spectra in their studies have a plateau before 10 MeV-cm²/mg and drop rapidly after 10 MeV-cm²/mg. In our case, the counts dropped quickly before 2 MeV-cm²/mg, and it became a straight line from 2 to 25 MeV-cm²/mg, followed by a long tail after 25 MeV-cm²/mg. To better understand the above-mentioned discrepancies, the y spectrum was separated by different contributors with various Z values.

For $y < 2$ MeV-cm²/mg, the major contributors are particles with $Z = 1$ and 2. As they are light ions, their contributions to LET spectra dropped sharply and disappeared for $y > 10$ MeV-cm²/mg.

For y between 2 and 10 MeV-cm²/mg, the contribution is mixed with low Z and high Z secondaries. In this region, contributions from low Z secondaries decrease sharply and high Z secondary particles became major contributors after $y > 5$ MeV-cm²/mg. These high Z secondaries were from heavy ions generated by (p, x) reactions. The y distribution of high Z secondaries had a peak around $y = 5$ MeV-cm²/mg with few counts in low y and a long tail in the high y region, extending to 50 to 60 MeV-cm²/mg.

Therefore, the overall y spectra of 200 MeV proton irradiated on silicon can be separated into three parts as follows. First part is $y < 2.5$ MeV-cm²/mg contributed from light ions; second part is 5 MeV-cm²/mg $< y < 10$ MeV-cm²/mg contributed by a mixture of both light and heavy ions and third part is $y > 10$ MeV-cm²/mg contributed only by heavy ions. In contrast to the works of Schwank et al. and Hiemstra et al. [8,40], the LET spectra of their studies have a cut off around 15–16 MeV-cm²/mg but not in our study.

This difference of our work and their work is because Schwank and Hiemstra used a reference Table to calculate the LET from energy fluence instead of calculating the energy deposition, and such method is only applicable for large target where the number of interactions is large enough that y can convergence to a single value which is LET. Unfortunately, in tiny SV, the y distribution is quite board when the SV is thin and using single expected value of LET becomes meaningless. Moreover, the reference Table used in their study has the cut off around 15–16 MeV-cm²/mg.

The differential fluences for LET < 5 MeV-cm²/mg are significantly different between our results and those of Hiemstra et al. [8]. In Figure 7 of Hiemstra’s work. the differential fluence is around 3000/10¹⁰ incident protons at LET = 1 MeV-cm²/mg and 1000/10¹⁰ at 5 MeV-cm²/mg. However, in our study, the differential fluence is 2400/10¹⁰ at 1 MeV-cm²/mg and 360/10¹⁰ at 5 MeV-cm²/mg as shown in the Figure 4. The slope in our study is about twice that of the Hiemstra’s result because Hiemstra et al. did not consider the light secondaries such as protons and helium. In our study, the γ contribution from each specific secondary particle is separate recorded, and they are plotted in Figure 5, where the proton and helium contribute more than 99% of the events in the region of γ < 5 MeV-cm²/mg.

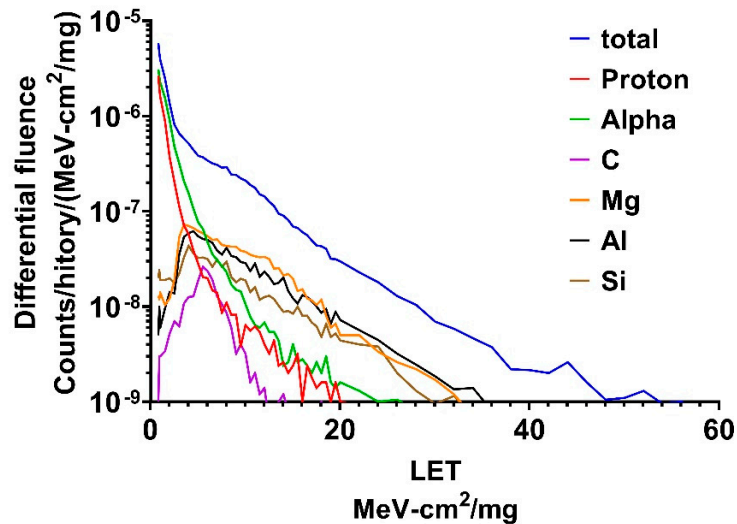


Figure 5. γ spectra in 100 nm silicon irradiated by a 200 MeV proton beam.

In previous SEEs studies, LET was usually treated as a single value for each incident particle with specific kinetic energy. However, Schrimpf et al. [4] and Shaneyfelt et al. [5] presented that, in some cases, LET versus SEEs cross-section is not a one to one function. In other words, the SEEs cross-section sometimes has large variation even though the LET is the same. In Table 1, the calculated LET of each type of secondary particle via the mean of its kinetic energy are listed. The calculation is done by two commonly used tools, namely LET124 and SRIM. LET124 is from the Tandem Van de Graaff Accelerator Facility at Brookhaven National Laboratory’s and SRIM is from Ziegler et al. [7].

Table 1. The calculated LET using mean energy of secondary particles generated by 200 MeV proton irradiate on silicon.

Z #	Mean Energy (MeV)	LET (LET124) * (MeV-cm ² /mg)	LET (SRIM-2013) ** (MeV-cm ² /mg)
2	5.32	0.5949	0.588
3	2.83	1.878	2.134
4	3.00	3.003	3.138
5	1.93	4.292	4.197
6	1.53	5.118	4.853
7	2.84	6.41	6.006
8	3.66	7.416	7.126
9	3.85	8.381	8.162
10	4.60	9.358	8.172
11	3.55	9.69	8.544
12	2.76	9.684	8.186
13	1.98	8.616	6.748
14	1.20	6.719	5.973

* Calculated by LET124 from Tandem Van de Graaff Accelerator Facility, Brookhaven National Laboratory, USA. ** Calculated by SRIM [9].

In the Table 1, even though both calculations are based on Bethe stopping formula but with different correction factor, the results can have more than 20% difference. When we look back to Figure 5, which plots the y in the SV for each kind of secondary particles, the y is not a single value or a symmetric distribution such as Gaussian distribution. Instead, the distribution is focus on low y region and has a very long tail in high y region. Take $Z = 12$ which is magnesium for example, the calculated LET is around $7 \text{ MeV}\cdot\text{cm}^2/\text{mg}$, but the maximum y can be larger than $50 \text{ MeV}\cdot\text{cm}^2/\text{mg}$, which is seven times higher than the mean. Therefore, using single value LET to estimate the SEEs is risky because the LET can only present the low y region, but the event which contribute SEEs can mostly from the high y tail. Due to the counts in high y region is quite less as compared to low y region, it has only little effect on the mean but may have significant effect on SEEs cross-section.

3.3. Effect of Various Physics Models on Secondary Yields

Raine and Jay et al. showed that the displacement damage in silicon from single particle interaction is dependent on the secondary particles type and energy deposition [41–43]. In this study, we also investigate if different physics models may affect the secondary particle yield. Figure 6 shows the secondary particle yields using various intra-nuclear cascade models in Geant4, and their comparison to Hiemstra's results [8]. The Hiemstra results come very close to the results of using the Bertini model. However, the peak in $Z = 6$ in this study was much higher than that from Hiemstra's result. In Hiemstra's study, all the secondary particles are from primary proton and they were calculated by the LAHET code system using Bertini cascade model. In the LET calculation part, Hiemstra's study did not consider the decay and further nuclear interaction. In our study, the primary proton will generate the first filial and first filial can still has a nuclear interaction and decay to generate the second or further filial. That is, a heavier secondary particle ($Z = 12, 13, \text{ or } 14$) may break into two middle-sized fragments ($Z = 6$) during its transportation as also shown by McNulty's result [44].

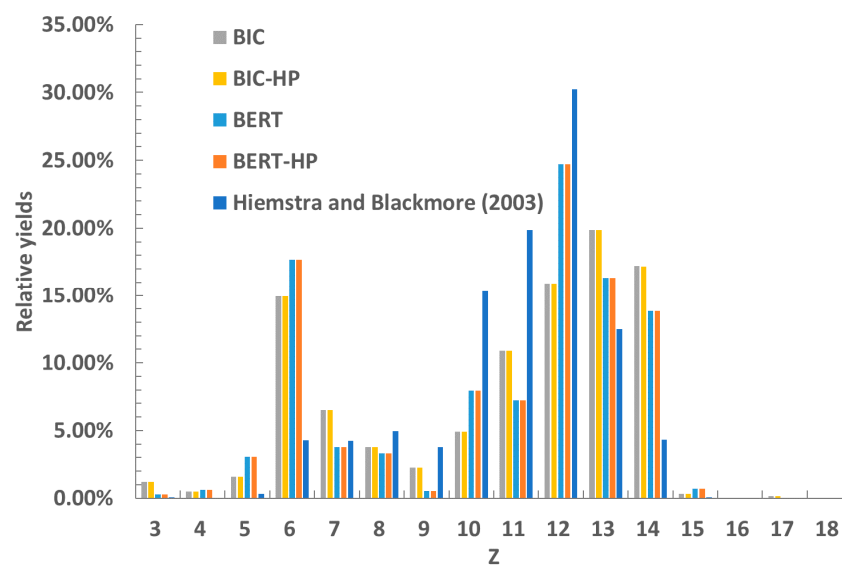


Figure 6. Secondary particle yields in 100 nm silicon irradiated by a 200 MeV proton beam using various physics models. BIC represents the Binary cascade model. BERT represents Bertini cascade model. HP represents high precision add-on.

Compared to the differences between the binary and the Bertini cascade, it is difficult to say that they are systematically different in Figure 6 and measurements are needed. In addition, for 10^9 incident particles, the high-precision physical model in Geant4 gave a negligible difference in secondary particle yields.

4. Conclusions

The concept of LET has been used to evaluate the Single Event Effect of radiation on semiconductor devices. In this work, we demonstrated that the conventional use of single value of LET is no longer applicable when the device dimension is scaling down to nano-material range. Instead, microdosimetry concept where the distribution of lineal energy will be necessary. We also performed a detailed microdosimetry Monte Carlo simulation of secondary particles from protons irradiating on silicon, and the results are shown to be very different from the previously reported work by Hiemstra and others with detail explanation. In particular, as compared to the simplified Monte Carlo results from Hiemstra [8], our results give much more low Z secondary particles which may not affect larger feature size but it will affect feature in nano-meter scale [45]. However, this study only focuses on a simplified hypothetical geometry. For realistic geometry, track structure technique should be used to estimate the geometrical distribution of energy deposition. Experimental verification of this difference will be our future work.

Author Contributions: Conceptualization, C.M.T. and T.-C.C.; methodology, C.-J.T. and C.-C.L.; Writing—original draft preparation, Y.C.; project administration, C.M.T.; writing—review and editing, C.M.T. and T.-C.C. All authors have read and agreed to the published version of the manuscript.

Funding: This research was funded by Taiwan Semiconductor Manufacturing Company JDP project. And Chang Gung Medical Research Program under projects CIRPD1I0021, BMRP736, CIRPD2F0024, and CIRPD2I0012.

Acknowledgments: This work was technically supported by the Particle Physics and Beam Delivery Core Laboratory of the Institute for Radiological Research, Chang Gung University/Chang Gung Memorial Hospital.

Conflicts of Interest: All authors have no conflict of interest to the organizations mentioned in the paper.

References

1. Garoli, D.; De Marcos, L.V.R.; Larruquert, J.I.; Corso, A.J.; Zaccaria, R.P.; Pelizzo, M.G. Mirrors for Space Telescopes: Degradation Issues. *Appl. Sci.* **2020**, *10*, 7538. [[CrossRef](#)]
2. Insoo, J. Effects of secondary particles on the total dose and the displacement damage in space proton environments. *IEEE Trans. Nucl. Sci.* **2001**, *48*, 162–175. [[CrossRef](#)]
3. Tan, F.; Huang, R.; An, X.; Wu, W.; Feng, H.; Huang, L.; Fan, J.; Zhang, X.; Wang, Y. Total ionizing dose (TID) effect and single event effect (SEE) in quasi-SOI nmOSFETs. *Semicond. Sci. Technol.* **2013**, *29*, 015010. [[CrossRef](#)]
4. Schrimpf, R.D.; Warren, K.M.; Weller, R.A.; Reed, R.A.; Massengill, L.W.; Alles, M.L.; Fleetwood, D.M.; Zhou, X.J.; Tsetseris, L.; Pantelides, S.T. Reliability and radiation effects in IC technologies. *IEEE Int. Reliab. Phys. Symp.* **2008**, 97–106. [[CrossRef](#)]
5. Shaneyfelt, M.R.; Schwank, J.R.; Dodd, P.E.; Felix, J.A. Total Ionizing Dose and Single Event Effects Hardness Assurance Qualification Issues for Microelectronics. *IEEE Trans. Nucl. Sci.* **2008**, *55*, 1926–1946. [[CrossRef](#)]
6. International Commission on Radiation Units and Measurements. *Linear Energy Transfer, in Report 16*; International Commission on Radiation Units and Measurements: Stockholm, Sweden, 2016; p. NP.
7. O'Neill, P.; Badhwar, G.; Culpepper, W. Risk assessment for heavy ions of parts tested with protons. *IEEE Trans. Nucl. Sci.* **1997**, *44*, 2311–2314. [[CrossRef](#)]
8. Hiemstra, D.; Blackmore, E. Let spectra of proton energy levels from 50 to 500 MeV and their effectiveness for single event effects characterization of microelectronics. *IEEE Trans. Nucl. Sci.* **2003**, *50*, 2245–2250. [[CrossRef](#)]
9. Ziegler, J.F.; Ziegler, M.; Biersack, J. SRIM—The stopping and range of ions in matter (2010). *Beam Interact. Mater. Atoms* **2010**, *268*, 1818–1823. [[CrossRef](#)]
10. Biersack, J.P.; Ziegler, J.F. The Stopping and Range of Ions in Solids. In *Ion Implantation Techniques*; Springer Nature: London, UK, 1982; pp. 122–156.
11. Dodd, P.; Shaneyfelt, M.; Felix, J.; Schwank, J. Production and propagation of single-event transients in high-speed digital logic ICs. *IEEE Trans. Nucl. Sci.* **2004**, *51*, 3278–3284. [[CrossRef](#)]
12. JEDEC Solid State Technology Association. *Test. Procedures for the Measurement of Single-Event Effects in Semiconductor Devices from Heavy Ion Irradiation, in JESD57A*; JEDEC Solid State Technology Association: Arlington, VA, USA, 2003.
13. Pickel, J.C. Single-event effects rate prediction. *IEEE Trans. Nucl. Sci.* **1996**, *43*, 483–495. [[CrossRef](#)]
14. Warren, K.M.; Weller, R.A.; Sierawski, B.D.; Reed, R.A.; Mendenhall, M.H.; Schrimpf, R.D.; Massengill, L.W.; Porter, M.E.; Wilkinson, J.D.; Label, K.A.; et al. Application of RADSAFE to Model the Single Event Upset Response of a 0.25 μm CMOS SRAM. *IEEE Trans. Nucl. Sci.* **2007**, *54*, 898–903. [[CrossRef](#)]

15. Warren, K.M.; Sierawski, B.D.; Reed, R.A.; Weller, R.A.; Carmichael, C.; Lesea, A.; Mendenhall, M.H.; Dodd, P.E.; Schrimpf, R.D.; Massengill, L.W.; et al. Monte-Carlo Based On-Orbit Single Event Upset Rate Prediction for a Radiation Hardened by Design Latch. *IEEE Trans. Nucl. Sci.* **2007**, *54*, 2419–2425. [[CrossRef](#)]
16. Bernal, M.A.; Bordage, M.-C.; Brown, J.; Davidkova, M.; Delage, E.; El Bitar, Z.; Enger, S.; Francis, Z.; Guatelli, S.; Ivanchenko, V.N.; et al. Track structure modeling in liquid water: A review of the Geant4-DNA very low energy extension of the Geant4 Monte Carlo simulation toolkit. *Phys. Medica* **2015**, *31*, 861–874. [[CrossRef](#)] [[PubMed](#)]
17. Incerti, S.S.; Baldacchino, G.; A Bernal, M.; Capra, R.; Champion, C.; Francis, Z.; Guèye, P.; Mantero, A.; Mascialino, B.; Moretto, P.; et al. THE GEANT4-DNA PROJECT. *Int. J. Model. Simul. Sci. Comput.* **2010**, *1*, 157–178. [[CrossRef](#)]
18. Incerti, S.; Ivanchenko, A.; Karamitros, M.; Mantero, A.; Moretto, P.; Tran, H.N.; Mascialino, B.; Champion, C.; Ivanchenko, V.N.; Bernal, M.A.; et al. Comparison of GEANT4 very low energy cross section models with experimental data in water. *Med. Phys.* **2010**, *37*, 4692–4708. [[CrossRef](#)]
19. Incerti, S.; Kyriakou, I.; Bernal, M.A.; Bordage, M.-C.; Francis, Z.; Guatelli, S.; Ivanchenko, V.; Karamitros, M.; Lampe, N.; Lee, S.B.; et al. Geant4-DNA example applications for track structure simulations in liquid water: A report from the Geant4-DNA Project. *Med. Phys.* **2018**, *45*, e722–e739. [[CrossRef](#)]
20. Hawkins, R.B. A microdosimetric-kinetic theory of the dependence of the RBE for cell death on LET. *Med. Phys.* **1998**, *25*, 1157–1170. [[CrossRef](#)]
21. Chiang, Y.; Tan, C.M.; Chao, T.-C.; Lee, C.-C.; Tung, C.-J. Investigate the Equivalence of Neutrons and Protons in Single Event Effects Testing: A Geant4 Study. *Appl. Sci.* **2020**, *10*, 3234. [[CrossRef](#)]
22. Dennis, J.A. Book review Microdosimetry. ICRU Report No. 36. pp. 118, 1983. (International Commission on Radiation Units and Measurements, Bethesda, Md.) \$18.00. *Br. J. Radiol.* **1985**, *58*, 250. [[CrossRef](#)]
23. Rossi, H.; Failla, G. Neutrons: Dosimetry. *Med. Phys.* **1950**, *2*, 603–607.
24. Rossi, H.H. Specification of Radiation Quality. *Radiat. Res.* **1959**, *10*, 522. [[CrossRef](#)]
25. Conte, V.; Colautti, P.; Grosswendt, B.; Moro, D.; De Nardo, L. Track structure of light ions: Experiments and simulations. *New J. Phys.* **2012**, *14*. [[CrossRef](#)]
26. Valentín, A.; Raine, M.; Sauvestre, J.-E.; Gaillardin, M.; Paillet, P. Geant4 physics processes for microdosimetry simulation: Very low energy electromagnetic models for electrons in silicon. *Beam Interact. Mater. Atoms* **2012**, *288*, 66–73. [[CrossRef](#)]
27. Ying, C.K.; Bolst, D.; Tran, L.T.; Guatelli, S.; Rosenfeld, A.B.; A Kamil, W. Contributions of secondary fragmentation by carbon ion beams in water phantom: Monte Carlo simulation. *J. Physics Conf. Ser.* **2017**, *851*, 012033. [[CrossRef](#)]
28. Foley, K.; Seifert, N.; Velamala, J.B.; Bennett, W.G.; Gupta, S.; Gupta, S. IRT: A modeling system for single event upset analysis that captures charge sharing effects. In Proceedings of the 2014 IEEE International Reliability Physics Symposium, Waikoloa, HI, USA, 1–5 June 2014; pp. 5F.1.1–5F.1.9.
29. Reed, R.A.; Weller, R.A.; Mendenhall, M.H.; Fleetwood, D.M.; Warren, K.M.; Sierawski, B.D.; King, M.P.; Schrimpf, R.D.; Auden, E.C. Physical Processes and Applications of the Monte Carlo Radiative Energy Deposition (MRED) Code. *IEEE Trans. Nucl. Sci.* **2015**, *62*, 1441–1461. [[CrossRef](#)]
30. Geant4-Collaboration. *Book for Application Developers, Rev 3.1 ed*; CERN: Geneva, Switzerland, 2019; p. 433.
31. Bertini, H.W. Intranuclear-Cascade Calculation of the Secondary Nucleon Spectra from Nucleon-Nucleus Interactions in the Energy Range 340 to 2900 MeV and Comparisons with Experiment. *Phys. Rev.* **1969**, *188*, 1711–1730. [[CrossRef](#)]
32. Folger, G.; Ivanchenko, V.N.; Wellisch, J.P. The Binary Cascade. *Eur. Phys. J. A* **2004**, *21*, 407–417. [[CrossRef](#)]
33. Wright, D.H.; Koi, T.; Folger, G.; Ivanchenko, V.; Kossov, M.; Starkov, N.; Heikkinen, A.; Wellisch, H. Low and High Energy Modeling in Geant4. In Proceedings of the Fourth Huntsville Gamma-Ray Burst Symposium; AIP Publishing: Melville, NY, USA, 2007; Volume 896, pp. 11–20.
34. Wright, D.H.; Kelsey, M.H. The Geant4 Bertini Cascade. *Nuclear Instruments and Methods. Accel. Spectrometers Detect. Assoc. Equip.* **2015**, *804*, 175–188. [[CrossRef](#)]
35. Koning, A.; Rochman, D. Modern Nuclear Data Evaluation with the TALYS Code System. *Nucl. Data Sheets* **2012**, *113*, 2841–2934. [[CrossRef](#)]
36. Otuka, N.; Dupont, E.; Semkova, V.; Pritychenko, B.; Blokhin, A.; Aikawa, M.; Babykina, S.; Bossant, M.; Chen, G.; Dunaeva, S.; et al. Towards a More Complete and Accurate Experimental Nuclear Reaction Data Library (EXFOR): International Collaboration Between Nuclear Reaction Data Centres (NRDC). *Nucl. Data Sheets* **2014**, *120*, 272–276. [[CrossRef](#)]
37. Agency, N.E. Joint Evaluated Fission and Fusion (JEFF) Nuclear Data Library. 6 March 2019. Available online: <https://www.oecd-nea.org/dbdata/jeff/> (accessed on 23 July 2019).
38. Horiowitz, Y.S.; Dubi, A. A proposed modification of Burlin’s general cavity theory for photons. *Physics Med. Biol.* **1982**, *27*, 867–870. [[CrossRef](#)]
39. Inguibert, C.; Duzellier, S. SEU rate calculation with GEANT4 (comparison with CREME 86). *IEEE Trans. Nucl. Sci.* **2004**, *51*, 2805–2810. [[CrossRef](#)]
40. Schwank, J.; Shaneyfelt, M.; Baggio, J.; Dodd, P.; Felix, J.; Ferlet-Cavrois, V.; Paillet, P.; Lambert, D.; Sexton, F.; Hash, G.; et al. Effects of particle energy on proton-induced single-event latchup. *IEEE Trans. Nucl. Sci.* **2005**, *52*, 2622–2629. [[CrossRef](#)]
41. Raine, M.; Jay, A.; Richard, N.; Goiffon, V.; Girard, S.; Gaillardin, M.; Paillet, P. Simulation of Single Particle Displacement Damage in Silicon—Part I: Global Approach and Primary Interaction Simulation. *IEEE Trans. Nucl. Sci.* **2016**, *64*, 133–140. [[CrossRef](#)]

42. Jay, A.; Raine, M.; Richard, N.; Mousseau, N.; Goiffon, V.; Hemeryck, A.; Magnan, P. Simulation of Single Particle Displacement Damage in Silicon—Part II: Generation and Long-Time Relaxation of Damage Structure. *IEEE Trans. Nucl. Sci.* **2017**, *64*, 141–148. [[CrossRef](#)]
43. Jay, A.; Hemeryck, A.; Richard, N.; Martin-Samos, L.; Raine, M.; Le Roch, A.; Mousseau, N.; Goiffon, V.; Paillet, P.; Gaillardin, M.; et al. Simulation of Single-Particle Displacement Damage in Silicon—Part III: First Principle Characterization of Defect Properties. *IEEE Trans. Nucl. Sci.* **2018**, *65*, 724–731. [[CrossRef](#)]
44. McNulty, P.J.; Farrell, G.E.; Tucker, W.P. Proton-Induced Nuclear Reactions in Silicon. *IEEE Trans. Nucl. Sci.* **1981**, *28*, 4007–4012. [[CrossRef](#)]
45. Bagatin, M.; Gerardin, S.; Paccagnella, A.; Visconti, A.; Virtanen, A.; Kettunen, H.; Costantino, A.; Ferlet-Cavrois, V.; Zadeh, A. Single Event Upsets Induced by Direct Ionization from Low-Energy Protons in Floating Gate Cells. *IEEE Trans. Nucl. Sci.* **2016**, *64*, 464–470. [[CrossRef](#)]